Solid State Syntheses of $12SrO \cdot 7Al_2O_3$ and Formation of High Density Oxygen Radical Anions, O^- and O_2^-

Katsuro Hayashi,*,† Naoto Ueda,‡ Satoru Matsuishi,§ Masahiro Hirano,§ Toshio Kamiya,‡ and Hideo Hosono‡,§

Secure Materials Center, Materials and Structures Laboratory, and, Frontier Research Center, Tokyo Institute of Technology, R3-34, Yokohama 226-8503, Japan

Received March 6, 2008. Revised Manuscript Received July 24, 2008

A new synthetic route via a solid-state reaction, the crystal structure of $12SrO \cdot 7Al_2O_3$ ($S_{12}A_7$) incorporated with OH^- ions, and the formation of oxygen radical anions in $S_{12}A_7$ have been examined. Investigations using X-ray powder diffraction and thermogravimetric and evolved gas combined analyses demonstrate that homogenization promoted by molten $Sr(OH)_2$ hydrates and the presence of Sr-hydrogarnet precursors play crucial roles in the formation of $S_{12}A_7$. Rietveld analyses confirm the lattice framework of $S_{12}A_7$ has a structure identical to that of the nanoporous crystal $12CaO \cdot 7Al_2O_3$ ($C_{12}A_7$, a mayenite structure) and demonstrate that two Sr^{2+} ions (pole Sr^{2+} ions) on the S_4 axis of a cage displace toward the cage center owing to the accommodation of an OH^- ion. An electron paramagnetic resonance study demonstrates that oxygen radical anions, O_2^- and O^-, are generated in the cages with concentrations on the order of 10^{20} cm^{-3} each by oxygen annealing. From the *g*-values observed at 77 K, the oxygen radical anions are interpreted as being sandwiched between the two pole Sr^{2+} ions rather than adsorbed on one side.

1. Introduction

$12CaO \cdot 7Al_2O_3$ ($C_{12}A_7$) is commonly known as the natural mineral "mayenite" as well as a constituent of calcium aluminate cements.[1] Although $C_{12}A_7$ appears to be useful only for structural material purposes, its unique nanostructure embedded in a crystal lattice has huge potential for exhibiting active functionalities as described later. In this study, we report a new synthetic route, crystal structure, and oxygen radical anion formation for $S_{12}A_7$,[2] which, as we will demonstrate, has a crystal structure identical to that of $C_{12}A_7$.

The crystal structure of $C_{12}A_7$ was determined in the early 1970s.[3] An incomplete network of AlO_4 tetrahedra incorporated with Ca^{2+} ions forms a cage structure. It is convenient to describe its unit cell composed of two formula units ($Z = 2$) as $[Ca_{24}Al_{28}O_{64}]^{4+} \cdot 2O^{2-}$. The $[Ca_{24}Al_{28}O_{64}]^{4+}$ component denotes the lattice framework containing 12 cages. Each cage has an inner free space of ~0.4 nm in diameter, and hence, only a mean effective charge of $+1/3|e|$ ($= +4|e|/12$ cages, where e is the elemental charge) is assigned to each. The remaining two O^{2-} ions do not belong to the framework, but randomly occupy 1/6 of the inner cage sites and are thereby referred to as "free oxygen" or "extra-framework oxide ions". The presence of the extra-framework O^{2-} ions is most likely an origin of the fast oxide ion conduction observed in a dry and oxidative atmosphere.[4,5] Furthermore, substitution of OH^-,[6,7] F^-, and Cl^- [8] for the O^{2-} ion is possible up to maximum occupancy, 1/3 of the total number of the cage sites. These monovalent anions and the O^{2-} ion have been believed to form continuous solid solution between the end members.

Incorporation of chemically unstable, that is, "active", anionic species into the cage by suitable chemical processes can render $C_{12}A_7$ a functional material. For example, thermal annealing in oxygen atmospheres generates highly reactive oxygen radical anions, O^- and O_2^-, in the cages up to nearly maximum occupancy. Their formation process,[9] thermodynamics,[10] molecular dynamics,[11] and extraction to vacuum

* Corresponding author. Phone: +81 + 45-924-5337. Fax: +81-45-924-5350. E-mail: k-hayashi@lucid.msl.titech.ac.jp.
† Secure Materials Center.
‡ Materials and Structures Laboratory.
§ Frontier Research Center.

(1) *Calcium Aluminate Cements 2001*; Mangabhai, R. J., Glasser, F. P. Eds.; IOM Communications, London, 2001.
(2) In this paper, we use the term "$S_{12}A_7$" to denote a crystalline phase that has a lattice framework composed of Sr and Al cations with a ratio of 12:14. The extra-framework anions are not specified, except those indicated in the text.
(3) Bartl, H. B.; Scheller, T. *Neues Jahrb. Miner. Monatsh* **1970**, *35*, 547.
(4) Lacerda, M.; Irvine, J. T. S.; Glasser, F. P.; West, A. R. *Nature* **1988**, *332*, 525.
(5) Irvine, J. T. S.; West, A. R. *Solid State Ionics* **1990**, *40/41*, 896.
(6) Nurse, R. W.; Welch, J. H.; Majumdar, A. *Trans. Br. Ceram. Soc.* **1965**, *64*, 323.
(7) Hayashi, K.; Hirano, M.; Hosono, H. *J. Phys. Chem. B* **2005**, *109*, 11900.
(8) Jeevaratnam, J.; Glasser, F. P.; Glasser, L. S. D. *J. Am. Ceram. Soc.* **1964**, *47*, 105.
(9) (a) Hosono, H.; Abe, Y. *Inorg. Chem.* **1987**, *26*, 1192. (b) Hayashi, K.; Hirano, M.; Matsuishi, S.; Hosono, H. *J. Am. Chem. Soc.* **2002**, *124*, 736. (c) Hayashi, K.; Hirano, M.; Li, Q.; Nishioka, M.; Sadakata, M.; Torimoto, Y.; Matsuishi, S.; Hosono, H. *Electorochem. Solid State Lett.* **2002**, *5*, J13. (d) Hayashi, K.; Matsuishi, S.; Ueda, N.; Hirano, M.; Hosono, H. *Chem. Mater.* **2003**, *15*, 1851. (e) Kajihara, K.; Matsuishi, S.; Hayashi, K.; Hirano, M.; Hosono, H. *J. Phys. Chem. C* **2007**, *111*, 14855.
(10) (a) Hayashi, K.; Matsuishi, S.; Hirano, M.; Hosono, H. *J. Phys. Chem. B* **2004**, *108*, 8920. (b) Hayashi, K.; Ueda, N.; Hirano, M.; Hosono, H. *Solid State Ionics* **2004**, *179*, 89. (c) Hayashi, K.; Hirano, M.; Hosono, H. *Br. Chem. Soc. Jpn.* **2007**, *80*, 872.
(11) Matsuishi, S.; Hayashi, K.; Hirano, M.; Tanaka, I.; Hosono, H. *J. Phys. Chem. B* **2004**, *108*, 8920.

10.1021/cm800666p CCC: $40.75
Published on Web 09/13/2008

as an O^- ion beam[12] have been studied in detail. Heat treatments in hydrogen atmospheres form another kind of reactive anion, the hydride (H^-) ion, in the cages. The H^-incorporation affords light- or electron-beam-induced insulator−conductor conversions.[13] Furthermore, "$C_{12}A_7$ electride"[14−17] is available by eliminating the extra-framework anions, leading to electron occupation in the free space of the cages. In the highly electron-doped electride, metallic[16] and superconducting[17] states have been achieved. Furthermore, several possible applications have been proposed for the electron-doped $C_{12}A_7$.[18]

The crystal structures of $C_{12}A_7$ with stoichiometric composition (i.e., O^{2-}-occupied[3,19−22]); partially O^{2-}-deficient;[21,22] and fully incorporated with OH^-,[20] F^-,[23] or electrons[16] have been studied in detail. According to the crystal symmetry, each cage has S_4 symmetry along an axis passing through two Ca^{2+} ions (pole Ca^{2+} ions) and the center of the cage (see Figure 1). It has been found that the anion incorporation in a cage causes a deformation of the local lattice geometry owing mainly to inward displacement of the pole Ca^{2+} ions of the corresponding cage. The displacement is less equivalent and more significant if the cage contains a divalent O^{2-} ion, as compared with monovalent anions.[20,22] This trend has also been predicted by theoretical study[24] and interpreted to be dependent principally on the strength of Coulomb attraction between the extra-framework anions and the pole cations, for which the cage inner side is not screened by the framework O^{2-} ions. In contrast, the cage geometry of fully electron-doped $C_{12}A_7$ is homogeneous, suggesting the electron densities for the cages are equivalent.[16]

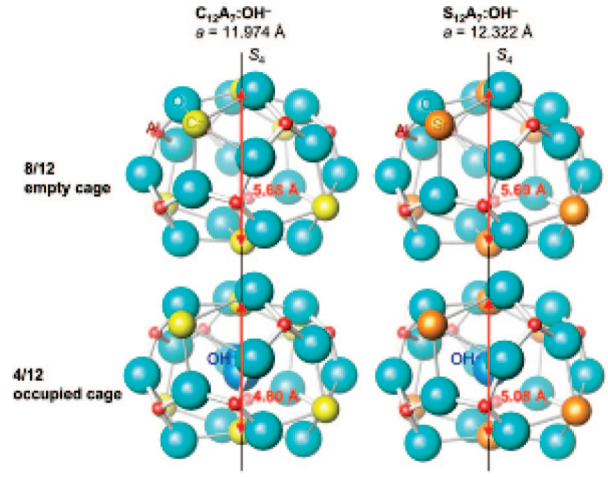

Figure 1. Structure of empty and OH^- ion-occupied cages for $C_{12}A_7$ (see ref 20) and $S_{12}A_7$.

Most previous works concerning $C_{12}A_7$-related materials have focused on the modification of extra-framework anions. For further exploration of functionalities and deeper understanding of these materials, modification of the cation site is also an important concern. So far, only a few publications have reported on cation substitutions. Irvine and West[5] examined the partial replacement of Al by Zn and P as a change in the content of extra-framework O^{2-} ions and a concomitant change in the oxide ionic conductivity. The unit cell of this system is represented as $[Ca_{24}(Al_{28-2x-2y}Zn_{2x}P_{2y})O_{64}]^{(4-2x+4y)+}\cdot(2-x+2y)O^{2-}$. A single phase was obtained in the composition field around $0 < x < 0.6$ and $0 < y < 0.4$. Feng et al.[25] synthesized $C_{12}A_7$ derivatives containing extra-framework Cl^- ions to an extent that necessitates extensive substitution of Si^{4+} for $A1^{3+}$ to preserve the charge neutrality. The unit cell is represented as $[Ca_{24}(Al_{28-x}Si_x)O_{64}]^{(4+x)+}\cdot(4+x)Cl^-$, where the maximum value of x is 6.8. Thus, the unit cell contains up to 10.8 Cl^- ions, which corresponds to the Cl occupancy in a cage of up to 0.9. Later, a new natural mineral, wadalite, was found in Japan and confirmed to have an identical crystal structure to and nearly the same chemical composition[26] as the material synthesized by Feng et al. Possible formation of a dechloridized form of wadalite with an ideal chemical composition $[Ca_{24}Al_{20}Si_8O_{64}]^{12+}\cdot 6O^{2-}$ (namely, oxywadalite) was claimed several years ago.[27] Electron paramagnetic resonance analysis of the oxywadalite powder detected a signal of O_2^- radicals that are, however, apparently situated in a different environment from the inner cage of $C_{12}A_7$. Raman bands observed at 1075 and 853 cm^{-1} have been assigned to O_2^- and O_2^{2-} ions, respectively. As for the

(12) (a) Li, Q.; Hayashi, K.; Nishioka, M.; Kashiwagi, H.; Hirano, M.; Torimoto, Y.; Hosono, H.; Sadakata, M. *Appl. Phys. Lett.* **2002**, *80*, 4259. (b) Nishioka, M.; Nanjyo, H.; Hamakawa, S.; Kobayashi, K.; Sato, K.; Inoue, T.; Mizukami, F.; Sadakata, M. *Solid State Ionics* **2006**, *177*, 2235.
(13) (a) Hayashi, K.; Matsuishi, S.; Kamiya, T.; Hirano, M.; Hosono, H. *Nature* **2002**, *419*, 462. (b) Hayashi, K.; Toda, Y.; Kamiya, T.; Hirano, M.; Yamanaka, M.; Tanaka, I.; Yamamoto, T.; Hosono, H. *Appl. Phys. Lett.* **2005**, *86*, 22109. (c) Matsuishi, S.; Hayashi, K.; Hirano, M.; Hosono, H. *J. Am. Chem. Soc.* **2005**, *127*, 12454. (d) Hayashi, K.; Sushko, P. V.; Shluger, A. L.; Hirano, M.; Hosono, H. *J. Phys. Chem. B* **2005**, *109*, 11900.
(14) Matsuishi, S.; Toda, Y.; Miyakawa, M.; Hayashi, K.; Hirano, M.; Tanaka, I.; Hosono, H. *Science* **2003**, *301*, 626.
(15) Miyakawa, M.; Toda, Y.; Hayashi, K.; Hirano, M.; Kamiya, T.; Matsunami, N.; Hosono, H. *J. Appl. Phys.* **2005**, *97*, 023510.
(16) Kim, S.-W.; Matsuishi, S.; Nomura, T.; Kubota, Y.; Takata, M.; Hayashi, K.; Kamiya, T.; Hirano, M.; Hosono, H. *Nano Lett.* **2007**, *7*, 1138.
(17) Miyakawa, M.; Kim, S.-W.; Hirano, H.; Kohama, Y.; Kawaji, H.; Atake, T.; Ikegami, H.; Kono, K.; Hosono, H. *J. Am. Chem. Soc.* **2007**, *129*, 7270.
(18) (a) Toda, Y.; Matsuishi, S.; Hayashi, K.; Ueda, K.; Kamiya, T.; Hirano, M.; Hosono, H. *Adv. Mater.* **2004**, *16*, 685. (b) Toda, Y.; Kim, S.-W.; Hayashi, K.; Hirano, M.; Kamiya, T.; Hosono, H.; Haraguchi, T.; Yasuda, H. *Appl. Phys. Lett.* **2005**, *87*, 254103. (c) Buchammagari, H.; Toda, Y.; Hirano, M.; Hosono, H.; Takeuchi, D.; Osakada, K. *Org. Lett.* **2007**, *9*, 4287.
(19) Boysen, H.; Lerch, M.; Stys, A.; Senyshyn, A. *Acta Crystallogr.* **2007**, *B63*, 675.
(20) Nomura, T.; Hayashi, K.; Kubota, Y.; Takata, M.; Kamiya, T.; Hirano, M.; Hosono, H. *Chem. Lett.* **2007**, *36*, 902.
(21) Palacios, L.; De La Torre, A. G.; Bruque, S.; García-Munõz, J. L.; García-Granda, S.; Sheptyakov, D.; Aranda, M. A. G. *Inorg. Chem.* **2007**, *46*, 4167.
(22) Palacios, L.; Cabeza, A.; Bruque, S.; García-Granda, S.; Aranda, M. A. G. *Inorg. Chem.* **2008**, *47*, 2661.
(23) Williams, P. P. *Acta Crystallogr.* **1973**, *B29*, 1550.
(24) (a) Sushko, P. V.; Shluger, A. L.; Hayashi, K.; Hirano, M.; Hosono, H. *Appl. Phys. Lett.* **2005**, *86*, 92101. (b) Sushko, P. V.; Shluger, A. L.; Hayashi, K.; Hirano, M.; Hosono, H. *Phys. Rev. B* **2006**, *73*, 045120. (c) Hayashi, K.; Sushko, P. V.; Muñoz Ramo, D.; Shluger, A. L.; Watauchi, S.; Tanaka, I.; Matsuishi, S.; Hirano, M.; Hosono, H. *J. Phys. Chem. B* **2007**, *111*, 1946.
(25) Feng, Q.; Glasser, F. P.; Alan-Howie, R.; Lachowski, E. E. *Acta Crystallogr.* **1988**, *C44*, 589.
(26) Tsukimura, K.; Kanazawa, Y.; Aoki, M.; Bunno, M. *Acta Crystallogr.* **1993**, *C49*, 205.
(27) (a) Fujita, S.; Suzuki, K.; Ohkawa, M.; Mori, T.; Iida, Y.; Miwa, Y.; Masuda, H.; Shimada, S. *Chem. Mater.* **2003**, *15*, 225. (b) Fujita, S.; Ohkawa, M.; Suzuki, K.; Nakano, H.; Mori, T.; Masuda, H. *Chem. Mater.* **2003**, *15*, 4879. (c) Mochizuki, K.; Hirabayashi, D.; Kojima, Y.; Suzuki, K. *J. Jpn. Inst. Metals* **2007**, *71*, 103.

substitution of the Ca sites, partial substitution of Mg up to the composition $[Ca_{22}Mg_2Al_{24}O_{64}]^{4+} \cdot 2O^{2-}$ has been examined.[28]

Full substitution of a cation site was found for the first time in a study by Yamaguchi et al.[29] They fabricated $S_{12}A_7$ by using a sol−gel precursor made of metal alkoxides and sintering its hydrolyzed product at 900 °C. The $S_{12}A_7$ phase is not found in the equilibrium phase diagram of the $SrO-Al_2O_3$ pseudobinary system,[31] and is presumably a quasi-stable phase. Indeed, they observed that further heating over 1040 °C led to decomposition into $3SrO \cdot Al_2O_3$ (S_3A) and $SrO \cdot Al_2O_3$ (SA) phases. They indexed observed reflections in X-ray diffraction (XRD) data assuming the same crystal structure as for $C_{12}A_7$ and then obtained the lattice constant 12.325 Å at room temperature. Very recently, Miyakawa et al. [30] fabricated $S_{12}A_7$ thin films by depositing amorphous $S_{12}A_7$, followed by annealing in humidified air at 840 °C. The crystallized phase has also been consistently indexed on the basis of the same crystal structure. Furthermore, the film was doped with H^- ions and electrons in the same manner as for $C_{12}A_7$ films,[15,17] supporting the presence of the cage structure in $S_{12}A_7$. However, crystal structure parameters (e.g., coordinates of atoms) of $S_{12}A_7$ have not yet been determined.

In this study, we develop a solid-state reaction method that uses cheaper raw materials and is suitable for larger-scale production, as compared with the metal alkoxide process. It is confirmed using Rietveld analysis that $S_{12}A_7$ has the same crystal structure as does $C_{12}A_7$. As indirect proof of the presence of cage structures, the accommodation of OH^- ions and oxygen radical anions, O_2^- and O^-, inside the cages is investigated. Similarities and differences between $S_{12}A_7$ and $C_{12}A_7$ are discussed in terms of crystal structures and geometry of the extra-framework anions.

2. Experimental Section

2.2. Exploration of $S_{12}A_7$ Formation Condition. The formation of $S_{12}A_7$ was examined using various combinations of Sr and Al sources: SrO (Kojyundo Chemical Co. Ltd. Japan, purity of 3N), $SrCO_3$ (Kojyundo, 3N), $Sr(OH)_2 \cdot 8H_2O$ (Kojyundo, 2N), $Al(OH)_3$ (Kojyundo, 3N), and γ-Al_2O_3 (Kojyundo, 3N). Stoichiometric or slightly Sr-rich amounts of these chemicals were mixed in a mortar with ethanol as a solvent until the solvent completely evaporated. The mixing of SrO or $Sr(OH)_2 \cdot 8H_2O$ with the Al source and the subsequent drying were carried out in an inert atmosphere to prevent the formation of $SrCO_3$ by a reaction with CO_2 in an ambient atmosphere.

A mixture of $SrCO_3$ and $Al(OH)_3$ was also prepared by the coprecipitation method to improve the homogeneity. Details of the process are as follows. A stoichiometric amount of metallic Al (Kojyundo, 4N) and $SrCO_3$ (Kojyundo, 3N) were dissolved in 1 N nitric acid. Ammonia−water (1.5 N) and 0.5 N ammonium carbonate aqueous solutions were added to the nitric solution so that the pH dropped to around 9. Sr^{2+} and Al^{3+} ions in the solution then precipitated as $SrCO_3$ and $Al(OH)_3$. The mixture of the precipitants was washed with distilled water and dried in an ambient atmosphere.

Table 1. Starting Mixture, Reaction Condition, and Resultant Product[a]

mixture	temp (°C)	time (h)	atmosphere	main phases
$SrCO_3 + Al(OH)_3$	800	6	ambient air	$S_3A + SA$
	900	6	ambient air	$S_3A + SA$
	1000	6	ambient air	$S_3A + SA$
$SrCO_3 + Al(OH)_3$ (coprecipitation)	800	6	ambient air	$S_3A + SA$
	900	6	ambient air	$S_3A + SA$
	1000	6	ambient air	$S_3A + SA$
$SrCO_3 + \gamma$-Al_2O_3	600	12	ambient air	$S_3A + SA$
	600	12	dry air	$S_3A + SA$
	600	12	wet N_2	$S_3A + SA$
	800	6	ambient air	$S_3A + SA$
	900	6	ambient air	$S_3A + SA$
	1000	6	ambient air	$S_3A + SA$
$SrO + \gamma$-Al_2O_3	600	12	ambient air	$S_3A + SA$
	800	6	ambient air	$S_3A + SA$
	1000	6	ambient air	$S_3A + SA$
$Sr(OH)_2 \cdot 8H_2O + Al(OH)_3$	600	12	ambient air	$S_{12}A_7$
	800	6	ambient air	$S_{12}A_7$
	900	6	ambient air	$S_{12}A_7$
	1000	6	ambient air	$S_3A + SA$
$Sr(OH)_2 \cdot 8H_2O + \gamma$-$Al_2O_3$	600	12	ambient air	$S_{12}A_7$
	700	6	ambient air	$S_{12}A_7$
	800	6	ambient air	$S_{12}A_7$
	800	6	dry air	$S_{12}A_7$
	800	6	wet N_2	$S_{12}A_7$
	900	6	ambient air	$S_{12}A_7$
	1000	6	ambient air	$S_3A + SA$

[a] In all batches, mixtures were cold isostatically pressed, heated at 200 $K \cdot h^{-1}$, and quenched after reaction.

Each mixture was uniaxially pressed into pellets with a diameter of 20 mm and a thickness of ~3 mm under a pressure of ~20 MPa. Some pieces of the pellets were further isostatically pressed under a pressure of 200 MPa using a cold isostatic pressing (CIP) machine. In an alumina tube furnace, these pellets were heated at a rate of 50 or 200 $K \cdot h^{-1}$ to temperatures between 600 and 1000 °C, kept for 6 or 12 h, and subsequently furnace-cooled or quenched to room temperature by transferring the product to a cooled zone quickly. The effect of the reaction atmosphere was examined for ambient air; dry air; and "wet" atmosphere, in which water vapor pressure $p(H_2O)$ was maintained at 0.02 atm by N_2 gas flow after passing through a humidifier.[7] Examined Sr−Al mixtures and reaction conditions are listed in Table 1.

2.3. Powder XRD Analysis. XRD patterns were collected at 298 K on a Rigaku RINT-2000 diffractometer using graphite-monochromated Cu Kα radiation. For phase identification and quantitative analyses, XRD patterns of diffraction angle, 2θ, between 10 and 70° were collected with a scan speed of 5° min^{-1}. For Rietveld analyses, X-ray data at diffraction angles between 10 and 140° in 0.02° steps were collected with a counting time of 5 s per step. The structural parameters were refined employing the RIETAN-2000 program.[32] Atomic scattering factors for Ca^{2+}, Al^{3+}, and O^- ions were used, and isotropic temperature factors were employed for all the atomic sites.

2.4. Thermogravimetric Analysis. The dynamic phase change and simultaneous gas phase emission during heating of the $Sr(OH)_2 \cdot 8H_2O-\gamma$-$Al_2O_3$ mixture were investigated by thermogravimetric, differential thermal, and evolved gas combined analyses (TG−DT−EGA) using a Rigaku Themoplus system. Wet N_2 carrier gas with $p(H_2O) = 0.02$ atm was supplied from the humidification

(28) Bertoni, M. I.; Mason, T. O.; Medvedeva, J. E.; Freeman, A. J.; Poepplmeier, K. R.; Delley, B. *J. Appl. Phys.* **2005**, *97*, 103713.
(29) Yamaguchi, O.; Narai, A.; Shimizu, K. *J. Am. Ceram. Soc.* **1986**, *69*, C-36.
(30) (a) Miyakawa, M.; Ueda, N.; Kamiya, T.; Hirano, M.; Hosono, H. *J. Ceram. Soc. Jpn.* **2007**, *115*, 567. (b) The present paper is cited as ref 14 herein.
(31) Hanic, F.; Chemekova, T.; Yu., Udalov.; Yu., P. *Russ. J. Inorg. Chem.* **1979**, *24*, 260.
(32) Izumi, F.; Ikeda, T. *Mater. Sci. Forum* **2000**, *321−324*, 198.

system to a small alumina-tube furnace of the TG−DT−EGA system. The weight change and heat flow were recorded with elevation of the temperature from room temperature to 1300 °C at a heating rate of 200 $K \cdot h^{-1}$. To investigate the dynamic phase change during the heating, samples were quenched to room temperature by turning off the heater's power supply when the temperature reached programmed values, which were set at roughly 100 K intervals on quasi-plateau ranges of the temperature−weight relationship. Phase compositions of the quenched samples were analyzed by XRD analysis. Since gas emission from a sample is not measurable when supplying the wet carrier gas, TG−DT−EGA were also carried out under the same conditions, except pure, dry He gas was used as the carrier gas. Desorbed gases were sampled through a silica capillary and analyzed with a quadrupole mass spectrometer. TG−DT−EGA were also used for investigating the dehydration property of the $S_{12}A_7$ phase. For this experiment, a product of a $Sr(OH)_2 \cdot 8H_2O-\gamma$-$Al_2O_3$ mixture heated at 800 °C for 12 h and cooled in a furnace in wet N_2 was used. This sample consists of mainly $S_{12}A_7$ (a mass fraction of 96%; other phases were S_3A and SA).

2.5. Infrared Spectroscopy. The product of a $Sr(OH)_2 \cdot 8H_2O-\gamma$-$Al_2O_3$ mixture heated at 600 °C for 12 h and quenched to room temperature in air was used as an "as-prepared" sample, and consisted mainly of $S_{12}A_7$ (a mass fraction of more than 90%; other phases were S_3A and SA). Some of the as-prepared sample was further heated in dry O_2 atmosphere at 600 °C for 12 h with heating and cooling rates of 200 $K \cdot h^{-1}$. The as-prepared and oxygen-annealed samples were powdered and mixed with infrared-measurement grade KBr, and finally pelletized. Transmission optical spectra were measured using a Perkin-Elmer Spectrum One Fourier transform infrared (FT-IR) spectrometer at room temperature.

2.6. Electron Paramagnetic Spin Resonance. Parts of the as-prepared sample were heated in dry O_2 atmosphere at 600 or 900 °C for 1−172 h with heating and cooling rates of 200 $K \cdot h^{-1}$. Electron paramagnetic resonance (EPR) measurements were performed at 9.7 GHz (X-band) using a Bruker E580 spectrometer at 77 K. The spin concentrations in the samples were determined from the second integral of the spectra using $CuSO_4 \cdot 5H_2O$ as a standard. Saturation properties against the microwave power were examined in both the samples and the standard. Quantitative measurements were carried out in each linear microwave power range, where the signal intensity is proportional to the square root of the microwave intensity.

3. Results and Discussion

3.1. Formation of $S_{12}A_7$. According to the study of $S_{12}A_7$ formation from a sol−gel precursor,[29] $S_{12}A_7$ decomposes into S_3A and SA phases at 1040 °C. Thus, reaction temperatures of 1000 °C or below were examined in this study. Table 1 lists starting mixtures, reaction conditions and resultant main phases in the products. In all the listed batches, the mixtures were cold isostatically pressed (CIP), heated at 200 $K \cdot h^{-1}$, and quenched after reaction. $S_{12}A_7$ never formed as a main phase when $SrCO_3$ was used as a Sr source, irrespective of the type of Al source, the type of mixing method (mortar mixing or coprecipitation), or reaction atmosphere. Decomposition of pure $SrCO_3$ into SrO and CO_2 in an ambient atmosphere requires a temperature as high as 1100 °C; however, the presence of Al reactants decreased the reaction temperature of $SrCO_3$ to below 600 °C, although the main products were S_3A and SA phases. Another starting Sr source, SrO, gave results similar to those for $SrCO_3$. In contrast, $S_{12}A_7$ phase always formed in the reaction temperature range between 600 and 900 °C as a main phase accompanied by both S_3A and SA as minor phases when $Sr(OH)_2 \cdot 8H_2O$ was used as a Sr source. Since $Sr(OH)_2 \cdot 8H_2O$ spontaneously dehydrates to $Sr(OH)_2 \cdot 2H_2O$ even at room temperature when exposed to a dry atmosphere, the starting mixtures contained both states of $Sr(OH)_2$ hydrate, and thus, similar results are expected if $Sr(OH)_2 \cdot 2H_2O$ is used as the Sr source. As for the reaction atmosphere, it was possible to form $S_{12}A_7$ in ambient air, dry air, and wet N_2. Among the examined three atmospheres, the wet N_2 gave the best $S_{12}A_7$ yield. It is concluded that $Sr(OH)_2$ hydrates are crucial for the synthesis of $S_{12}A_7$ via a solid state reaction route.

Table 2. Effects of the Sr/Al Ratio in the Starting Mixture, Cold Isostatic Press, and Heating Condition[a]

				weight ratio		
no.	Sr/Al	CIP	heating ($K \cdot h^{-1}$)	S_3A	$S_{12}A_7$	SA
1	12:14	yes	50	0.15	0.74	0.11
2	12:14	yes	200	0.06	0.91	0.03
3	12:14	no	50	0.39	0.28	0.33
4	12:14	no	200	0.11	0.81	0.08
5	12.12:14	no	200	0.10	0.86	0.05
6	12.24:14	no	200	0.07	0.92	0.01

[a] In all batches, $Sr(OH)_2 \cdot 8H_2O-\gamma$-$Al_2O_3$ mixtures were heated at 800 °C for 6 h in a wet N_2 atmosphere.

Table 2 summarizes the effects of other reaction parameters on the yield of $S_{12}A_7$ formation. In all experiments, mixtures of $Sr(OH)_2 \cdot 8H_2O$ and γ-Al_2O_3 were heated at 800 °C for 6 h in wet N_2 atmosphere. By comparing the results of conditions 1 and 2 with those of 3 and 4, it is found that CIP slightly improves the yield. The effect of the heating rate can be determined from a comparison of conditions 1 and 3 with 2 and 4. Decreasing the heating rate to 50 $K \cdot h^{-1}$ markedly worsens the yield. In the experiments for conditions 4, 5, and 6, the effect of the Sr/Al ratio (stoichiometric to $S_{12}A_7$ or a slightly Sr-rich composition) in the starting mixtures was examined. Paradoxically, as the deviation from the stoichiometric cation ratio increased, the yield of the $S_{12}A_7$ phase itself improved by the suppression of the CA formation. However, further deviation from the stoichiometric composition is expected to rather worsen the $S_{12}A_7$ yield owing to an increase in the S_3A portion.

Such an enigmatic preparation condition dependence of the $S_{12}A_7$ formation is likely to be due to its reaction route. To elucidate this, the dynamic phase change during the process of heating the $Sr(OH)_2 \cdot 8H_2O-\gamma$-$Al_2O_3$ mixture was investigated. TG−DT−EGA were used to survey key temperature regions for the reactions and concurrent gas phase emissions during the reactions. The dynamic phase change during the reaction was also investigated by XRD analysis for a series of the samples obtained by quenching at various temperatures. Results of TG−DTA are plotted in Figure 2a. Since the gas emission from a sample is not measurable when supplying the wet carrier gas, TG−DT−EGA were also carried out under the same conditions, except that dry He was substituted for the wet N_2. Water desorption in dry He is plotted in Figure 2b. It should be noted that TG curves for wet N_2 and dry He exhibited similar characteristics; a one-to-one correspondence was observed for the

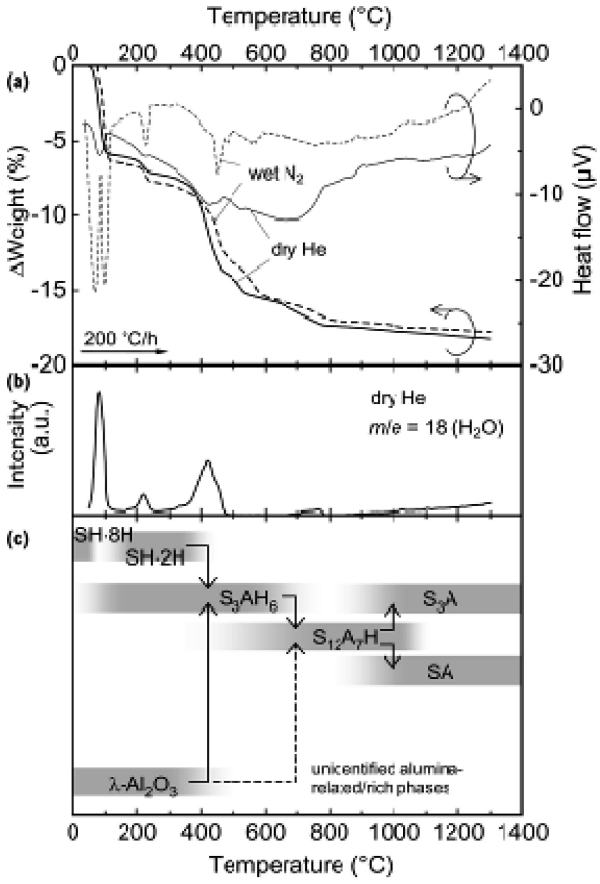

Figure 2. Thermogravimetric, differential thermal, and evolved gas combined analyses (TG−DT−EGA) and the dynamic phase change during heating of a $Sr(OH)_2 \cdot 8H_2O-\gamma$-$Al_2O_3$ mixture at a rate of 200 $K \cdot h^{-1}$. (a) TG−DT−EGA for wet N_2 and dry He atmospheres. (b) Water desorption in dry He atmosphere. (c) Main phases observed by XRD analysis. Sr-rich to Al-rich phases are presented from top to bottom. Abbreviations: $Sr(OH)_2 \cdot 8H_2O$ (SH·8H); $Sr(OH)_2 \cdot 2H_2O$ (SH·2H); $3SrO \cdot Al_2O_3 \cdot 6H_2O$ (S_3AH_6); $3SrO \cdot Al_2O_3$ (S_3A); $12SrO \cdot 7Al_2O_3 \cdot H_2O$ ($S_{12}A_7H$); $SrO \cdot Al_2O_3$ (SA).

temperature range and amount of weight loss, whereas the wet N_2 curve shifted to a higher temperature with respect to the dry He curve. This shift is ascribed to a difference in the equilibrium of water between the sample and atmosphere. From the correspondence of the two TG curves, water desorption in wet N_2 can be also be inferred from the desorption curve in dry He. Figure 2c is a dynamic phase diagram summarizing the main phases during heating at a rate of 200 $K \cdot h^{-1}$ in wet N_2.

The reaction for each temperature range is interpreted as follows. At around 100 °C, dehydration of $Sr(OH)_2 \cdot 8H_2O$ to $Sr(OH)_2 \cdot 2H_2O$ occurs, and $3SrO \cdot Al_2O_3 \cdot 6H_2O$ (Sr-hydrogarnet with a space group of $I\bar{a}3d$ and lattice constant of 11.285 Å[33]) begins to be formed. The Sr-hydrogarnet has the same crystal structure as a garnet, in which all anion sites are occupied by OH^- ions. Water desorption around 250 °C is probably triggered by the melting of $Sr(OH)_2$, whereas $Sr(OH)_2 \cdot 2H_2O$ was observed in the quenched samples up to ~400 °C. This suggests the melting point is the onset of the principal formation of the hydrogarnet, and its formation is nearly completed at ~400 °C. It is probable that the reaction is markedly promoted by the presence of the molten $Sr(OH)_2$. In this temperature range, γ-Al_2O_3 disappears; thus, some Al reacts to form the hydrogarnet. The situation for the remaining Al has not been clarified. Since X-ray atomic scattering for Al is small, its presence was not easily confirmed by XRD analysis. We speculate the remaining Al may form amorphous strontium−aluminate hydrates or other transitional phases, which are dispersed in a matrix of hydrogarnet. Large weight loss and water desorption at 400−500 °C is probably attributed to dehydration of the hydrogarnet and concurrent formation of $S_{12}A_7$. $S_{12}A_7$ was observed above 400 °C, and its formation was nearly completed at ~800 °C. $S_{12}A_7$ again emits water at ~1000 °C and decomposes into S_3A and SA. The water emission suggests $S_{12}A_7$ has a crystal structure that accommodates OH^- in a cage, as does $C_{12}A_7$. Thus, this hydrous $S_{12}A_7$ is indicated as $S_{12}A_7H$ in Figure 2c. The OH^- incorporation will be examined in detail in the next section. Resultant samples consisting of $S_{12}A_7$, S_3A, or SA are so stable that no degradation was observed when stored in laboratory air. In contrast, samples containing a large amount of the Sr-hydrogarnet phase exhibited efflorescence.

In conclusion, a key for the formation of $S_{12}A_7$ is the presence of a precursor phase, Sr-hydrogarnet, whose formation is likely enhanced by the melting of $Sr(OH)_2$ hydrates and the supply of OH^- ions. $S_{12}A_7$ is probably a quasi-stable phase that is stabilized by the accommodation of OH^- ions under a hydrous condition,[34] and its formation from the Sr-hydrogarnet has a kinetic advantage over the formation of S_3A and SA phases.

According to this interpretation, it is possible to explain the mysterious preparation condition dependences observed in our experiments. The $S_{12}A_7$ formation temperature range (400−800 °C) is not high enough to homogenize a local chemical composition in a sample by long-range diffusion or evaporation−precipitation. An inhomogeneity that has not been dissolved until the last stage of the reaction may lead to the formation of S_3A and SA phases. The starting material being made denser by CIP is advantageous in decreasing the diffusion length required for attaining certain homogeneity. Furthermore, the homogenization assisted by the molten $Sr(OH)_2$ hydrates becomes more effective in Sr-richer samples. As for the effect of the reaction atmosphere, CO_2 in ambient air may change the $Sr(OH)_2$ hydrates to $SrCO_3$, which does not contribute to the formation of the hydrogarnet, decreasing the $S_{12}A_7$ formation yield. In a dry atmosphere, $S_{12}A_7$ may decompose more easily by dehydration, again decreasing its yield. As for the experimental fact that a slower heating rate results in poorer yields, we speculate that $Sr(OH)_2$ hydrates tend to dehydrate before their conversion to the hydrogarnet, or the hydrogarnet dehydrates to convert into other phases before reaching the $S_{12}A_7$

(33) Nevskii, N. N.; Ivanov-Emin, B. N.; Nevskaya, N. A.; Kaziev, G. Z.; Belov, N. V. *Doklady Akademii Nauk SSSR* **1982**, *264*, 857.

(34) If the OH^- ion-incorporated $S_{12}A_7$ is assumed to be an equilibirum phase in the $SrO-Al_2O-H_2O$ pesudoternary system, then Gibbs' phase law allows the $S_{12}A_7$ phase to coexist in both S_3A and SA phases, even if the total Sr:Al ratio in the system is exactly 12:14. Higher $p(H_2O)$ may increase the equilibrium portion of $S_{12}A_7$ among the three phases. Even if our reaction condition was within the equilibirum phase field of $S_{12}A_7$, we suppose the amounts of residual S_3A and SA phases are still not determined by the equilibirum partition but determined by the inhomogeneity in the starting mixtures.

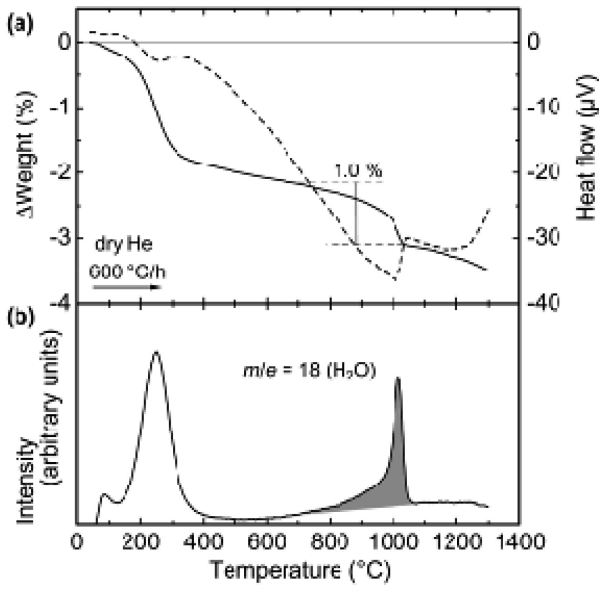

Figure 3. TG−DT−EGA of $Sr_{12}A_7$.

formation temperature. The absence of CIP possibly leads to similar results, because water desorption is easier in a less dense stating material.

3.2. Crystal Structure of $S_{12}A_7$. The highest yield of $S_{12}A_7$ was achieved in a batch different from those indicated in Table 1. $Sr(OH)_2 \cdot 8H_2O$ and γ-Al_2O_3 were carefully mixed and heated at 800 °C for 6 h in wet N_2, and this was followed by furnace cooling. Mass fractions of $S_{12}A_7$, S_3A, and SA in this sample estimated by Rietveld analysis were 96, 2, and 2%, respectively. The details of the analysis are described later. The surface area of the sample evaluated by the Brunauer−Emmet−Teller (BET) multiple point measurement[35] was $21 \pm 2\ m^2 \cdot g^{-1}$, which corresponds to an average grain diameter of ~80 nm. This size is comparable to that observed by scanning electron microscopy.[36]

To confirm the presence and quantify the amount of OH^- ion incorporated in $S_{12}A_7$, TG−DT−EGA were carried out on the sample. Figure 3 shows the results obtained in dry He atmosphere. There are three temperature ranges of weight loss accompanying water desorption. The filled area in Figure 3b is ascribed to water desorption due to dehydration of OH^- ions that were accommodated in $S_{12}A_7$. The concomitant weight loss between 700 and 1050 °C is estimated to be 1.0%, as indicated in Figure 3a. If it is assumed $S_{12}A_7$ has the same crystal structure as $C_{12}A_7$ has, the change in the chemical formula for a unit cell is described as

$$[Sr_{24}Al_{28}O_{64}]^{4+} \cdot OH^- \rightarrow [Sr_{24}Al_{28}O_{64}]^{4+} \cdot 2O^{2-} + H_2O(g) \quad (1)$$

The observed weight loss agrees well with the expected weight loss, 1.0%, and this supports that the cages in the obtained $S_{12}A_7$ sample are fully incorporated with OH^- ions. However, the occurrence of the fully anhydrous form ($[Sr_{24}Al_{28}O_{64}]^{4+} \cdot 2O^{2-}$) is unknown. As suggested by the observation of the sharp water desorption peak at 1000 °C, as the OH^- concentration decreases below a certain level, the crystal is no longer stable and decomposes into S_3A and SA phases simultaneously with water emission corresponding to the amount of residual OH^- ion.

Other water desorption peaks appear at ~100 and 250 °C. The former is most likely ascribed to physisorbed water on the surfaces. Its weight loss, 0.2%, corresponds to the adsorption of 0.4 layers of H_2O molecules, if the molecular size reported in the literature[37] is employed. The amount of physisorbed water may be reasonable. The latter peak at 250 °C is usually ascribed to chemisorbed water; that is, a H_2O molecule splits into a OH^- ion, which binds to a surface cation, and a proton, which forms another OH^- ion by binding to a surface O^{2-} ion. However, the amount of OH^- ion on the surfaces estimated from the weight loss, 1.5%, is 66 ions per cross-sectional area of the unit cell ($1.23 \times 1.23\ nm^2$). This value is impossible, because it far exceeds the number of atomic sites on the surface. We hypothesize that such a large amount of OH^- ion is stored as a hydrogarnet (-like) layer that forms on the $S_{12}A_7$ surface. The weight loss of 1.5% corresponds to hydrogarnet layers of 1.3 unit cell thickness. This hypothesis is supported by $S_{12}A_7$ ($\bar{I}43d$, 1.23 nm) and Sr-hydrogarnet[33] ($I\bar{a}3d$, 1.13 nm) having similar crystal structures and lattice constants, and thereby each crystal is possibly grown (semi-) epitaxially on another. If such crystallographic similarity facilitates the interconversion of the two phases, it is convincing that the hydrogarnet phase acts as a "seedbed" of $S_{12}A_7$ formation in the synthesis.

Since the result of TG−DT−EGA supported the chemical composition of $[Sr_{24}Al_{28}O_{64}]^{4+} \cdot 4OH^-$ for the as-prepared $S_{12}A_7$ sample, this chemical composition and the crystal structure identical to $C_{12}A_7$ were employed in Rietveld analysis. Figure 4 shows the measured XRD data and the fitting result of Rietveld analysis. All the diffractions ascribed to $S_{12}A_7$ are consistently indexed using the space group $\bar{I}43d$, indicating the incorporation of OH^- ions has no ordering. According to this space group, each cage has S_4 symmetry along the axis passing through two Sr^{2+} ions (pole Sr^{2+} ions) and the center of the cage. Practically, this local symmetry may be preserved only approximately because the cages are distorted by extra-framework ions.

The previous analysis of $[Ca_{24}Al_{28}O_{64}]^{4+} \cdot 4OH^-$ [20] demonstrated that the local distortion by the OH^- ion is well described by a combination of empty and OH^- ion-occupied deformed cages, where the pole Ca^{2+} ion is displaced inwardly along the S_4 axis by an attraction to the OH^- ion. To model this, the Ca site was split into two sites (Ca1 and Ca2), keeping the total occupancy of the two Ca sites as unity. In the case of the asymmetric cage deformation caused by the off-S_4 axis O^{2-} ion incorporation, this was more exactly depicted by a Rietveld model employing extra Ca and Al sites.[22] However, we employed the two-site splitting model (giving Sr1 and Sr2 sites) in the analysis of

(35) The BET measurement was carried out using Bel BELSORP-max volumetric adsorption equipment. The sample was pre-treated under reduced pressure ($<10^{-2}$ Pa) at ~300 °C for 2h. Without exposing the pretreated sample to ambient air, the adsorption isotherm of N_2 was measured at 77 K.

(36) Powdered sample was sprinkled on a carbon tape, and this was followed by sputtering of a Pt−Pd thin coating. A Hitachi S-4500 SEM was used for the observation.

(37) McClellan, A. L.; Harnsberger, H. F. *J. Colloid Interface Sci.* **1967**, *23*, 577.

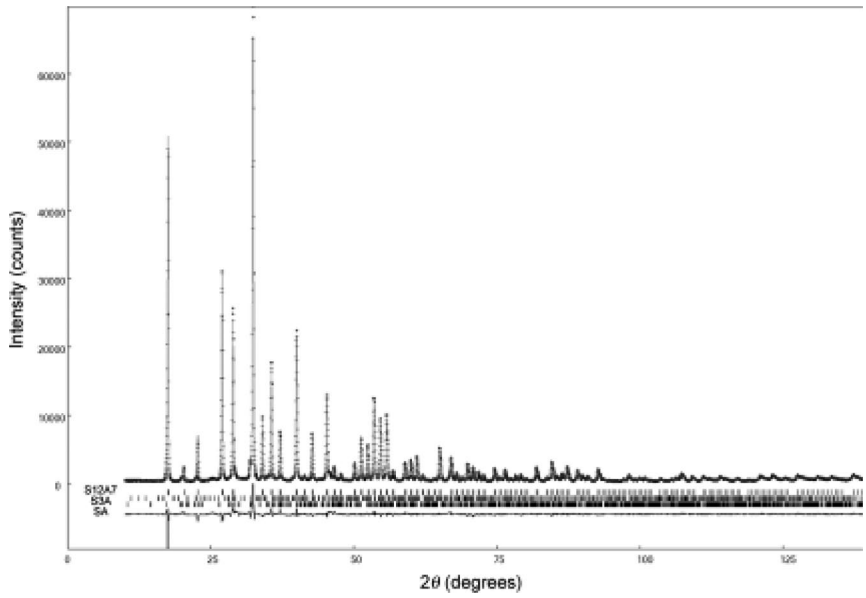

Figure 4. Experimental XRD pattern and fitting result of three phase Rietveld analysis incorporating $S_{12}A_7$, S_3A, and SA phases.

Table 3. Refined Structure Parameters for Hydroxy-Strontium-Maynite at 298 K.

formula			$(SrO)_{12} \cdot (Al_2O_3)_7 \cdot H_2O$ ($Z = 2$)			
space group			$I\bar{4}3d$ (No. 220)			
lattice constant (Å)			12.3220(4)			
theoretical density ($g \cdot cm^{-3}$)			3.503			
site	Wyckoff	x	y	z	g	B ($Å^2$)
Sr1	24*d*	0. 1442(1)	0	1/4	2/3	0.72(1)
Sr2	24*d*	0. 1688(3)	0	1/4	1/3	= Sr1[b]
Al1	16c	0. 0166(1)	= x	= x	1	0.56(2)
Al2	12*b*	7/8	0	1/4	1	= Al1[b]
O1	48*e*	0.1482(2)	0.9616(2)	0.0440(2)	1	0.63(5)
O2	16*c*	0.9418(2)	= x	= x	1	= O1[b]
O3[a]	12*b*	3/8	0	1/4	1/3	= O1[b]
R factors (%)			R_I, 4.27; R_{WP}, 7.27			
delected interatomic distances (Å)			Sr1−Sr1, 5.688(3); Sr2−Sr2, 5.083(9); O3−O1, 3.336(3)			
atomic displacement (Å)			Sr1−Sr2: 0.303(6)			

[a] Hydrogen bound to O3 oxygen was omitted. [b] These constraints are employed for a stable convergence in the analysis.

$[Sr_{24}Al_{28}O_{64}] \cdot 4OH^-$ because a structure that is analogous to the $[Ca_{24}Al_{28}O_{64}]^{4+} \cdot 4OH^-$ is most feasible, and this model has the OH^- ion at the cage center as described below. In fact, the incorporation of the two site splitting reasonably improved the R factors.[38] The OH^- ion was allocated to the O3 site, and the proton was neglected because it has almost no sensitivity in XRD. First, the O3 site was allocated to the 24*d* site, which is on the S_4 axis. The O3 position converged to the cage center. However, the estimated error for the O3 position was larger than the size of the cage, suggesting a large statistical displacement of OH^- from the cage center or a technical problem in the analysis: a strong correlation to the neighboring heavy atoms. Thus, the OH^- position was fixed at the cage center; that is, the 12*b* site. The final result is given in Table 3. Sr1−Sr1 and Sr2−Sr2 distances were 5.69 and 5.08 Å, respectively, indicating the pole Sr^{2+} ions were displaced toward the cage center owing to the accommodation of OH^- and their distance was shortened by 0.30 Å with respect to that for an empty cage. Half the Sr2−Sr2 distance, 2.54 Å, agrees well with the sum (2.56 Å) of the ionic radii of Sr^{2+} (1.16 Å[39]) and O^{2-} (1.40 Å[39]), again supporting the presence of an OH^- ion at the cage center. The crystal structure of $[Sr_{24}Al_{28}O_{64}] \cdot 4OH^-$ is confirmed to be identical to that of $[Ca_{24}Al_{28}O_{64}] \cdot 4OH^-$.

Structures of empty and OH^--occupied cages in $[Ca_{24}Al_{28}O_{64}] \cdot 4OH^-$ and $[Sr_{24}Al_{28}O_{64}] \cdot 4OH^-$ are illustrated in Figure 1. Distances between the pole cations in the empty cages are nearly the same in both crystals, whereas those in occupied cages differ only by the difference in the ionic radii of the pole cations. Nevertheless, the OH^- ion in $S_{12}A_7$ appears to be more tightly sandwiched because of less tolerance in the displacement span of the pole cations. The OH^- ion at the cage center is surrounded by three types of O^{2-} ion sites: (i) the O1 site (bridging oxygen) not coordi-

(38) For example, if Sr1 and Sr2 were again unified to one Sr site and the other parameters were kept the same as in the analysis corresponding to Table 3 and Figure 4. The Rietveld fitting gave worse R factors ($R_I = 4.27$ and $R_{WP} = 7.98$) and abnormally large thermal parameters for the Sr site ($B = 1.25$ Å^2). As for the occupancies of Sr1 and Sr2 sites, an appropriate convergence was not achieved when these values were not fixed. Since they strongly correlate with their fraction coordinates and thermal parameters, they are most sensitively affected by the quality of the sample. We set these occupancies as ideal values.

(39) Shannon, R. D. *Acta Crystallogr.* **1976**, *A32*, 751.

(40) The hydrogen bond between the OH^- ion and the framework O^{2-} ion causes a deviation in the OH^- position from the cage center. Thus, each O−H···O distance in a OH^--incorporated cage may be shorter by a few tenths of an angstrom than that (3.23 Å) evaluated using the statistical center position determined by Rietveld analysis.

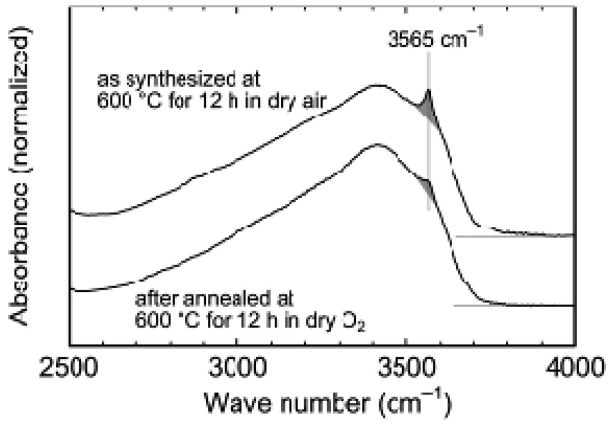

Figure 5. Transmission infrared spectra for $S_{12}A_7$ powder samples dispersed in KBr.

nated to the pole Sr^{2+} ions, (ii) the O1 site coordinated to the pole Sr^{2+} ions, and (iii) the O2 site (nonbridging oxygen) coordinated to the pole Sr^{2+} ions. The distance (3.34 Å) from the OH^- ion is shortest for the first ion type among the three.[34] Thus, the OH^- ion likely forms a very weak hydrogen bond at this type of O^{2-} ion. The type of nearest oxygen is the same as that in $C_{12}A_7$.

3.3. Incorporation of Oxygen Radicals. Since $S_{12}A_7$ has the same crystallographic features as $C_{12}A_7$ has, it is expected that oxygen radical anions, O_2^- and O^-, can also be generated inside the cages of $S_{12}A_7$. This section describes a study on the oxygen radical anions incorporated as a substitute for the OH^- ions by annealing in a dry oxygen atmosphere.

The product of a $Sr(OH)_2 \cdot 8H_2O - \gamma\text{-}Al_2O_3$ mixture heated at 600 °C for 12 h and quenched to room temperature in ambient air was used as an as-prepared sample, and consists of mainly $S_{12}A_7$ (a mass fraction greater than 90%; other phases were S_3A and SA). Some of the as-prepared sample was further heated in a dry O_2 atmosphere at 600 °C for 12 h with heating and cooling rates of 200 K·h^{-1}. These samples kept the same $S_{12}A_7$ mass fraction. Figure 5 shows infrared spectra for the as-prepared and O_2-annealed samples. Since the O−H stretching band of the extra-framework OH^- ion in $C_{12}A_7$ has been observed in the range 3540−3555 cm^{-1},[7] peaks at 3565 cm^{-1} in Figure 5 are also assigned to the extra-framework OH^- ion in $S_{12}A_7$. The shift in wavenumber is ascribed to the fact that the hydrogen bond between the extra-framework OH^- and the framework O^{2-} ion in $S_{12}A_7$ is longer by ~0.1 Å than that in $C_{12}A_7$. It is also found in Figure 5 that the amount of OH^- ion markedly decreased with dry oxygen annealing.

The as-prepared samples were heated in a dry O_2 atmosphere at 600 or 900 °C for 1−172 h with heating and cooling rates of 200 K·h^{-1}. Figure 6 shows typical EPR spectra measured at 77 K and their simulation. The spectrum of the as-prepared sample (Figure 6a) is well-reproduced by a powder pattern for O_2^- with Lorentzian line shapes and g values of $g_{xx} = 2.003$ (±0.001), $g_{yy} = 2.006$ (0.001), and $g_{zz} = 2.065$ (0.001). Its concentration was below 1×10^{18} cm^{-3}. After the oxygen annealing, the total spin concentration markedly increased, and another signal was superposed on

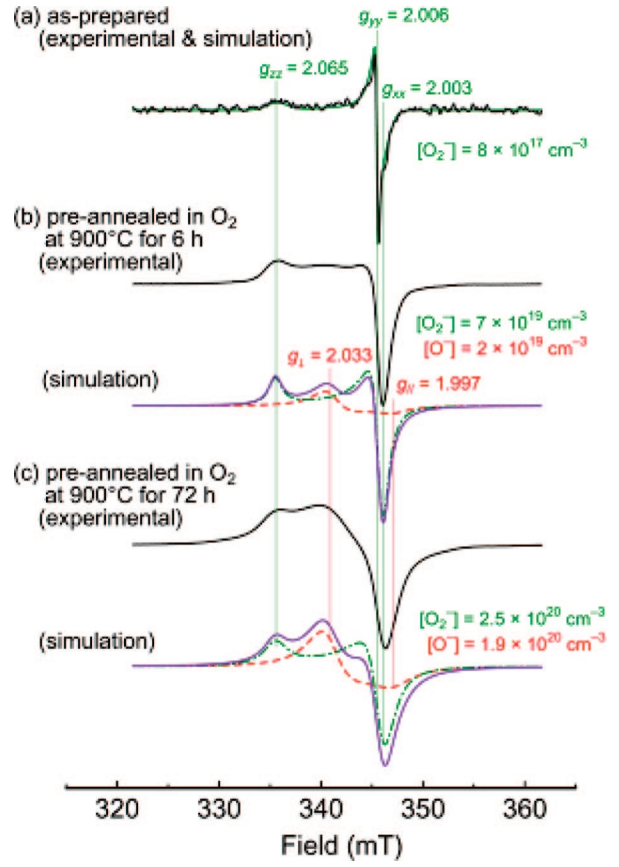

Figure 6. EPR powder pattern of O_2^- and O^- in $S_{12}A_7$. (a) O_2^- in as-prepared $S_{12}A_7$. Optimized line widths are $\sigma_{zz} = 20$, $\sigma_{yy} = 2$, and $\sigma_{xx} = 15$ Gauss. (b, c) O_2^- and O^- superposed spectra in oxygen annealed $S_{12}A_7$. In the simulation of the two spectra, anisotropy in line width was not optimized. Concentrations of O^- and O_2^- were evaluated from the intensity ratio of a calculated spectrum giving the best fit to a measured one.

the O_2^- signal. As found in Figure 6b and c, all spectra for the annealed samples were consistently reproduced by an additional signal having $g_\perp = 2.035$ (0.002) and $g_{//} = 1.997$ (0.01), which are assumed to be independent of the radical concentrations. These observations are very similar to those in the $C_{12}A_7$ case.[9,11] Thus, the additional signal is assigned to O^-. The absence of resolved hyperfine splitting due to ^{27}Al (I = 5/2, abundance of 100%) supports that O_2^- and O^- radical anions are not incorporated in the lattice framework but are accommodated inside the cages. As for ^{87}Sr (I = 9/2, abundance of 7.0%) nuclear, the apparent absence of the hyperfine lines in the measured spectra is explained by ionic bonds between the pole Sr^{2+} ions and the extra-framework radical anions. The intensity of each hyperfine line becomes negligibly small owing to the split into many hyperfine lines and the low natural abundance.

The observed g values for oxygen radical anions in $S_{12}A_7$ are compared with those in $C_{12}A_7$ in Table 4. Differences in the environment of oxygen radical anions will be discussed in terms of the observed g values.

The interaction of an O_2^- ion with a cation splits the degenerated π_g orbital into two components with an energy separation, Δ. Usually, the x-axis is taken along the half-occupied π_g orbital (denoted as π_g^x), y along the fully

Table 4. Relationship between Parameters for Lattice Framework and Extra-Framework Anions

		O_2-annealed $C_{12}A_7$		fully hydrated $C_{12}A_7$	O_2-annealed $S_{12}A_7$	fully hydrated $S_{12}A_7$
temp (K)		4.2	77	298	77	298
O3−O1 (Å)				3.23[a]		3.34
OH stretch (cm^{-1})				3540−3555[b]		3565
Ca1−Ca1 or Sr1−Sr1(Å)				5.68[c]		5.69
Ca2−Ca2 or Sr2−Sr2 (Å)				4.80[c]		5.08
O_2^-	g_{xx}	2.002(1)[d]	2.002(1)[d]		2.003(1)	
	g_{yy}	2.009(1)[d]	2.008(1)[e]		2.006(1)	
	g_{zz}	2.081(1)[d]	2.074(1)[d]		2.065(1)	
O^-	$g_{//}$		1.994(10)[e]		1.997(10)	
	$g_{\perp}$		2.036(5)[e]		2.033(5)	

[a] Calculated from CIF data provided in ref 20. [b] Ref 7. [c] Ref 20. [d] Ref 11. [e] Ref 9.

occupied π_g orbital (π_g^y), and z along the internuclear axis. Approximated theoretical equations for the g tensor are[41]

$$g_{xx} = g_e \quad g_{yy} = g_e + \frac{2\lambda}{E} \quad g_{zz} = g_e + \frac{2\lambda}{\Delta} \tag{2}$$

where g_e is the g value for a free electron, λ is the spin−orbit coupling constant of oxygen, and E is the energy separation between σ_g^z and π_g^x orbitals. The approximation is quite reasonable under the condition $\lambda < 0.10\Delta \ll E$. Equation 2 indicates g_{zz} is a sensitive reflection of the environment of the O_2^- ion. Indeed, there is a general trend that the g_{zz} value decreases with an increase in the oxidation state of the cation[41] owing to a larger interaction between O_2^- and the cation. Furthermore, the g_{zz} value decreases as the cation−O_2^- distance decreases. This trend has been confirmed both from experiments (e.g., g_{zz} values for O_2^- adsorbed on MgO, CaO, and SrO are ~2.08, 2.09, and 2.10[41]) and theoretical calculations.[42]

In a previous study,[11] it was established that an O_2^- ion in a $C_{12}A_7$ cage is adsorbed onto one of the pole Ca^{2+} ions with a side-on configuration at a low temperature. The resultant local crystallographic field with C_2 symmetry controls the favored internuclear direction. Observed g values are $g_{xx} = 2.002$, $g_{yy} = 2.009$, and $g_{zz} = 2.080$ at 4.2 K. Warming to 77 K changes the values to $g_{xx} = 2.002$ and $g_{zz} = 2.074$, and these values unify at ~2.04 at 220 K, whereas g_{yy} was found to remain nearly constant. This observation indicates that the molecular motion of O_2^- can be described by rotational swinging about the y-axis, which is perpendicular to the internuclear axis and parallel to the S_4 axis of the cage, below 220 K, and free rotation about the y-axis over 220 K.

As shown in Table 4, the lower g_{zz} value for $S_{12}A_7$ compared with $C_{12}A_7$ at 77 K is apparently contradictory to the greater ionic radius of the cation, 1.00 Å for Ca^{2+} as compared to 1.12 Å for Sr^{2+}, if it is assumed that an O_2^- ion adsorbs on one of the pole cations. Furthermore, the decrease in the g_{zz} value is not principally ascribed to its temperature-dependent downward shift due to enhanced rotational motion about the y-axis, since the g_{xx} value at 77 K is still close to the g_e value, implying the motion is not sufficiently intense to give a significant counter shift in g_{zz}. Therefore, we propose the position of O_2^- in the $S_{12}A_7$ cage is much closer to the cage center so that the O_2^- ion is sandwiched between the pole Sr^{2+} ions in the same manner that the OH^- ion is accommodated in a cage. This coordination strengthens the interaction between the π_g^y orbital and the cations, thereby shifting g_{zz} to a lower value. This idea is anticipated from a more tightly sandwiched OH^- ion in the $S_{12}A_7$ cage as compared with the $C_{12}A_7$ cage (see Figure 1). However, the absence of a marked difference between g_{xx} and g_e suggests rotational motion is still restrained by the local crystal field. It follows that the position of O_2^- is not exactly at the cage center, but still shifted toward one side, and the concurrent local C_2 symmetric crystal field controls the favored internuclear direction. Thus, displacement of the two pole Sr^{2+} ions to sandwich the O_2^- ion is rather asymmetric.

A simplified theoretical description of the g tensor for O^- for axial symmetry is[43]

$$g_{\perp} = g_{xx} = g_{yy} = g_e + \frac{2\lambda}{E'} \quad g_{//} = g_{zz} \cong g_e \tag{3}$$

where E' is the energy splitting between half-occupied p_z and degenerated fully occupied p_x and p_y levels. Two components of the g tensor ($g_{\perp}$) should exceed g_e, and the third should be less or equal to that of g_e according to a more exact formulation.[44] Similar to the case for O_2^-, the interaction between a cation and an adsorbed O^- ion has an important effect on the $g_{\perp}$value, which generally decreases with an increase in the cation charge[43] and a decrease in the cation-O^- distance. Adsorption of an O^- ion on one pole cation again cannot account for the $g_{\perp}$ value for $S_{12}A_7$ being smaller than that for $C_{12}A_7$. Thus, the O^- ion, as well as the O_2^- ion, in $S_{12}A_7$ is sandwiched by the two pole Sr^{2+} ions, the inward displacements of which are more symmetrical than those in $C_{12}A_7$, strengthening the cation−O^- interaction.

Figure 7 shows the change in oxygen radical anion concentrations against the time for preannealing in O_2. After preannealing, the samples were cooled at a rate of 200 $K \cdot h^{-1}$ in the same atmosphere. Analogous to the case for $C_{12}A_7$, the formation of oxygen radical anions is expected to involve two steps: First, the extra-framework O^{2-} ions are formed by dehydration as described in eq 1. The reaction of the O^{2-} ions and the excess oxygens absorbed from the atmosphere then generate the O_2^- and O^- ions in the cages.[9] For example, an equimolar formation of O_2^- and O^- is described as

$$O^{2-}(\text{cage}) + O_2(g) \rightarrow O^-(\text{cage}) + O_2^-(\text{cage}) \tag{4}$$

where "cage" denotes the species accommodated in the cage. The dehydration is promoted at a higher temperature,[7]

(41) Che, M.; Tench, A. J. *Adv. Catal.* **1983**, *32*, 1.
(42) Tatsumi, K.; Shiotani, M.; Freed, J. H. *J. Phys. Chem.* **1983**, *87*, 3425.
(43) Che, M.; Tench, A. J. *Adv. Catal.* **1982**, *31*, 77.
(44) Brailsford, J. R.; Morton, J. R.; Vannotti, L. E. *J. Chem. Phys.* **1968**, *49*, 2237.

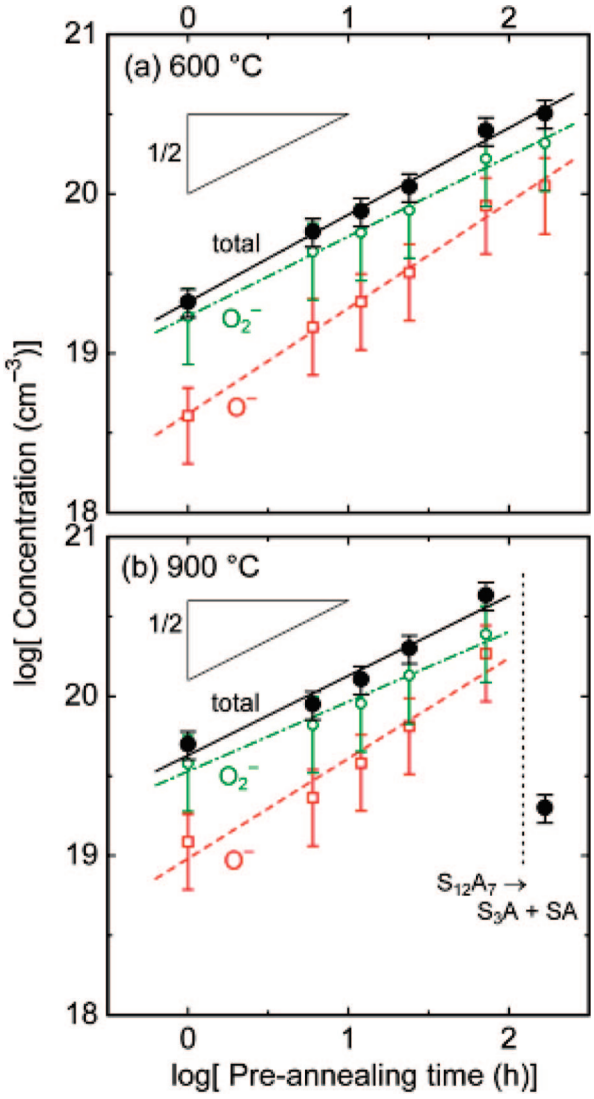

Figure 7. Concentrations of O_2^- and O^- plotted against preannealing time in O_2 at 600 °C (a), and 900 °C (b). After preannealing, samples were cooled at a rate of 200 K·h^{-1} in the same atmosphere. The concentration was evaluated by EPR.

whereas a lower temperature is advantageous for oxygen absorption to generate oxygen radical anions in terms of the chemical equilibrium. For example, the total radical concentration in $C_{12}A_7$ in equilibrium at 1 atm O_2 has been estimated to be 7×10^{19} cm^{-3} at 900 °C, increasing to 7×10^{20} cm^{-3} at 600 °C.[10] The results of Figure 7, therefore, suggest dehydration was enhanced for higher temperature or longer preannealing time, enhancing the formation of oxygen radical anions during the cooling process. The square-root dependence in the radical anion concentration−time relationship suggests that the rate determination process for the dehydration is the bulk diffusion of OH^- ions, and the resulting amount of extra-framework O^{2-} ion limits the final amount of oxygen radical anion. The decomposition of $S_{12}A_7$ phase during preannealing at 900 °C for 172 h is caused by a shortage of extra-framework OH^- ions, which are necessary to stabilize the $S_{12}A_7$ phase. Thus, the total radical anion concentration (several 10^{20} cm^{-3}) obtained just before decomposition is likely to be the maximum limit attainable by this annealing process, with all samples still having residual OH^- ions. The possibilities of forming fully oxygen radical anion-incorporated $[Sr_{24}Al_{28}O_{64}]^{4+}\cdot(4-x)O_2^-\cdot xO^-$ as well as anhydrous stoichiometric $[Sr_{24}Al_{28}O_{64}]^{4+}\cdot 2O^{2-}$ are still unclear.

4. Conclusions

Synthesis of $S_{12}A_7$ via a solid-state reaction is possible when $Sr(OH)_2$ hydrates and γ-Al_2O_3 or $Al(OH)_3$ are used as starting mixtures and reacted in a temperature range between 600 and 900 °C. In this process, homogenization promoted by molten $Sr(OH)_2$ hydrates and a kinetic advantage for Sr-hydrogarnet over S_3A and SA in the formation of $S_{12}A_7$ are likely to play crucial roles in achieving a higher yield of $S_{12}A_7$.

$S_{12}A_7$ has the same crystal structure as $C_{12}A_7$. Furthermore, the OH^- ion can be fully incorporated in $S_{12}A_7$, leading to the chemical composition $[Sr_{24}Al_{28}O_{64}]\cdot 4OH^-$. The interatomic distance between pole Sr^{2+} ions in an empty cage is nearly the same as that for $C_{12}A_7$, whereas the interatomic distance in an OH^--occupied cage is longer by the difference between the ionic radii of the pole cations.

It is possible to form oxygen radical anions, O_2^- and O^-, in the cages with concentrations on the order of 10^{20} cm^{-3} for each by heating OH^--incorporated $S_{12}A_7$ in a dry oxygen atmosphere. The observed g values suggest that oxygen radical anions in $S_{12}A_7$ are sandwiched between the two pole cations rather than adsorbed on one of the pole cations at a low temperature. The absence of enhanced rotational motion of O_2^- at a low temperature indicates that its molecular direction is still restricted by the local crystal field, suggesting the position of the O_2^- ion is not exactly at the cage center.

Acknowledgment. K.H. is supported by the Ministry of Education, Culture, Sports, Science and Technology (MEXT) of the Japanese Government under Grants-in-Aid of Scientific Research for Young Scientists (No. 19685019). T.K. is supported by MEXT under Grants-in-Aid of Scientific Research on Priority Areas (No. 19051007). H.H. is supported by MEXT under Grants-in-Aid of Creative Scientific Research (No. 16GS0205).

Note Added after ASAP Publication. The journal titles were incorrect in refs 21 and 22 in the version published ASAP September 13, 2008; the corrected version was published October 7, 2008.

Supporting Information Available: Crystallographic information files (CIF) for $S_{12}A_7H$. This material is available free of charge via the Internet at http://pubs.acs.org.

CM800666P